Materials Research. 2021; 24(suppl. 1): e20210007
DOI: https://doi.org/10.1590/1980-5373-MR-2021-0007

Deposition of TiO_2 thin Films by Dip-Coating Technique from a Two-Phase Solution Method and Application to Photocatalysis

***Luiz F. K. Pedrini*[a], *Lucas C. Escaliante*[a], *Luis V. A. Scalvi*[a,b*]**

[a]*Universidade Estadual Paulista, Faculdade de Ciências, Programa de Pós-graduação em Ciência e Tecnologia de Materiais, Bauru, SP, Brasil.*
[b]*Universidade Estadual Paulista, Escola de Ciências, Departamento de Física, Bauru, SP, Brasil.*

Received: January 9, 2021; Revised: May 31, 2021; Accepted: June 24, 2021

A derivation of the sol-gel-dip-coating deposition technique is proposed, where the precursor solution exhibits two separated liquid phases, reaching an equilibrium state in a heterogeneous solution. Structural, optical and photocatalytic properties of TiO_2 films grown from the proposed two phases method are shown and discussed, along with the properties of films deposited when the top phase present distinct lengths, which are observed through SEM images and optical transmittance spectra. The dominant crystalline phase is anatase for all the films prepared. Films are tested towards their efficiency for photocatalysis, using methylene blue as dye degradation agent. It has been found that films deposited through the two phase method are more efficient on the photocatalyitic degradation of methylene blue.

Keywords: *Dip-Coating, Sol-Gel, Titanium Dioxide, Photocatalysis.*

1. Introduction

Titanium dioxide (TiO_2) is a semiconductor oxide that has drawn attention due to its application in the creation of several sorts of devices. It is worth mentioning its role as photocatalyst for removal of air and water pollutants[1], but its applications have been studied in a variety of fields and in a multitude of sample forms. It may be used s gas-sensors[2,3] being doped with different elements[4-6] in solar cells[5,7] in prosthetics[8] besides the photocatalyst function itself[1,9,10]. To accomplish the goals of such a variety of applications, the knowledge on the properties and characteristics of this material are fundamental, and TiO_2 has a vast and well established literature available. TiO_2 has a wide bandgap between 3.0 and 3.8 eV depending on the crystal structure[11,12]. Anatase, crystal structure acquired most commonly through heat treatments below 700 °C[13], has an in direct bandgap of about 3.25 eV[14]. Rutile, the most thermodynamically stable structure[15], has a direct bandgap of around 3.0eV[14]. Other structures such as brookite, TiO_2 -B, baddeleyite and columbite are less focused on studies, either by a lack of known interesting properties or difficulty in their respective preparation[16,17].

The TiO_2 structure may be controlled as well as the crystallite average size, either by the thermal annealing temperature[18] or through the precursor solution's pH[19]. Among the possible applications of TiO_2, the research to apply its properties as a photocatalyst has been growing side by side with the increasing worry about water pollution and climate change[20,21]. The photocatalytic property of TiO_2 has been applied in a variety of ways to breakdown either CO_2 molecules[22] and complex carbon molecules in water[23-25], to increase potable water yield[26], or to break water molecules, producing hydrogen as a renewable energy source[27], being most commonly used in its anatase phase. Lowering the bandgap through doping[28], increasing surface area and reactivity through different deposition and growth methods[29] are some ways that have shown to increase TiO_2 photocatalytic efficiency.

Concerning the deposition of thin films, they have a variety of applications, in different areas of scientific and technological knowledge. Several methods for thin film preparation have been designed and used to achieve this diversity of applications, such as: epitaxial growth, resistive evaporation, chemical vapor deposition (CVD), atomic layer deposition (ALD), sol-gel methods (dip-coating, spin-coating and doctor blading) and Langmuir-Blodgett, among others.

From these techniques, sol-gel presents simplicity in the production of semiconductor oxide films at different size scales that other methods lack. Among the methods using sol-gel precursor solution, dip-coating is a well known method due to its cost and efficiency[29]. This deposition process may be separated into three stages: 1. immersion, where a substrate is immersed into a precursor solution at a constant rate, followed by a time interval in which the substrate remains submerged, interacting with the precursor solution; 2. deposition and drainage: when dragging the substrate out the container holding the precursor solution, at constant rate, part of the fluid that adheres to the substrate surface overcomes the surface tension of the solution and another part is drained back into the container, forming a thin layer of gel on the substrate surface; 3. evaporation: the solvent present in the deposited thin layer, adhered to the substrate, immediately begins to evaporate when exposed to air, leading to densification of the adhered material.

*e-mail: luis.scalvi@unesp.br

The rate of evaporation depends on atmospheric properties such as temperature, pressure and composition, and affects the resulting film structure and composition[30]. With a higher rate of evaporation, the densification, that starts with the aggregation of particles in the sol-gel and eventual gelation of those aggregates, happens faster, resulting in a more fragile and porous structure[13,31]. Heating the solution and consequently the film may result in further densification, but with a rapid loss of solvent the mobility of particles and interactions between the deposited solution and the substrate reduce drastically, possibly reducing the bonding strength between the aggregates and the substrate[13]. As a counterpoint, heating the substrate may have an opposite effect. Increasing the energy available to particles may increase the average length that the particles travel on the substrate surface, eventually bonding with deeper sites, creating stronger bonds. Santos et al.[32] found that substrates kept at higher temperature leads to higher optical transmittance in the near-infrared region, associated with a lower concentration of free electrons.

The most complex aspect, then, in the deposition process is the stability and composition of the precursor solution: initial reagents must be soluble in water or react and form products that are soluble in water. All molecules present in the solution, ligands, additives and surfactants must decompose during thermal annealing, and to maintain stability in the solution and allow deposition by wetting, counter ions and ligands must not deteriorate in order to control the wetting properties. The interaction of fluids and solid components makes the method interesting and complex from a theoretical point of view, and establishing direct relationships between the properties of precursor solutions and the properties of the final product is not a straightforward task.

In this work, aiming to increase the number of available parameters to better control and further develop the dip-coating method, the precursor solutions are prepared to reach equilibrium in the separation between two liquid phases. The proposed deposition system is outlined in Figure 1 and compared with the generally used method. Two-phase systems for dip-coating deposition process appear in the literature with Ceratti and coworkers[33] where the heterogeneous is investigated as a more efficient way of obtaining films, requiring a smaller volume of the precursor solution in the dip-coating process. Ceratti's method uses heavy liquids, such as perfluorodecaline, gallium or mercury, to maintain a thin liquid layer of the depositing precursor solution near the top of the container, forming the first phase with which the substrate interacts during deposition, allowing it to be fully wetted by the solution, without having to completely fill the container with the precursor solution. The method proposed here works in a reversed way: a less dense phase, without the presence of the material to be deposited (region A in Figure 1) floats on top of the precursor solution containing the material (region B in Figure 1) to be deposited. While the sol-gel solution is divided between A and B, film samples can be divided in 2 regions as well, denoted as I and II. While region I interacts only with the top phase (A), region II of film samples have interacted with both phases (A and B) during deposition.

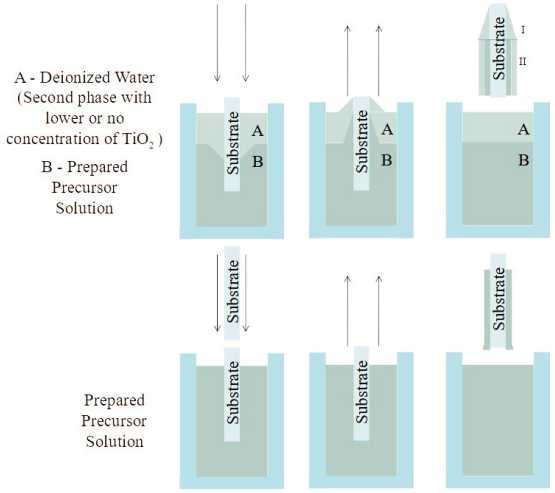

Figure 1. Proposed method (top) and conventional dip coating process (bottom). The label "A" refers to the floating (top) phase, whereas "B" refers to the denser (bottom) phase. The proposed method creates different regions in the sol-gel solution and deposited film.

It is possible to establish similarities of the present proposal with the Langmuir-Blodgett method[31] and with the method proposed by Ceratti[33] in the sense that, by changing the disposition of the material dispersed in the aqueous medium, it is possible to modify the interaction mechanisms between the particles and the medium, creating new structures and morphological properties in the deposited film. Besides, it has been shown that it can be more efficient than the conventional method, as proposed in the case of Ceratti's procedure. Similar methods to the proposed here are more commonly found for film formation from polymers[34-36]. As the methods are different, it is possible to compare the goals of this paper with Ceratti et al.'s[33]. In this paper the bi-phasic system is created to become a new parameter to be studied and to see its effects on the deposited films, and the "main" phase is the heavier, bottom one, different from the referenced work, where the material to be deposited is the higher one, which floats on top of a heavier, mostly inert liquid. Their goal was to validate their method as a way to reproduce films while being more efficient with solutions.

One of the goals of the presently proposed method, to more easily investigate its effects on the produced films, is to reduce and eliminate the concentration of TiO_2 in the upper phase (A). The development of two-phase systems for film deposition provides an opportunity to deal with disadvantages of the sol-gel-dip-coating method such as the stability of the medium, easily oxidized or dried, the difficulty in preparation of solutions or their viability to be used in larger scales. Thickness control can be accomplished through the deposition rate, but the range of possible thicknesses can be narrow depending on the sol-gel solution used, with thinner films requiring a slower deposition rate. Eventually thermal annealing or rapid evaporation of solvents can crack film's structures. The proposed method could eventually complement the process with advantages, such as: better control of thickness and homogeneity, isolation of the precursor solution from air for facilitated storage,

introduction of immiscible components, greater efficiency and possible new doping methods.

In this paper we use the two-phase sol-gel dip coating deposition to verify the optical and morphologic properties of deposited films with distinct heights of the top layer (A in Figure 1), and the efficiency of this process applied to photocatalysis, using methylene blue as degradation dye. Alongside the resulting effects achieved by the method in photocatalysis is the reduction of material deposited, thinner films without slowing down deposition rate, as well as increasing surface area with less material. The change in surface tension dynamics also allows for the change in draining regime without change in deposition rate, which lead to the formation of structures found mostly in samples under the evaporation regime at high deposition rate (10 cm/min). Lastly, the increase in photocatalytic efficiency when applying the method is tied to the increase in surface area, which, with a smaller volume of material deposited and thinner film is an interesting achievement.

2. Experimental

2.1. Preparation of TiO_2 colloidal suspensions

The proposed method for preparing precursor solutions was developed through derivation of the method used by Hanaor et al.[37] and Trino et al.[38]. The amounts needed for the preparation of 50 mL of the precursor solution is as follows: 185.0 mL of deionized water, 56.7 mL of isopropanol ($CH_3CHOHCH_3$), 2.6 mL of Nitric acid (HNO_3), and 15 mL of titanium isopropoxide (TTIP). In a beaker, deionized water and isopropanol are mixed, and the content is magnetically stirred while the acid is added slowly. Then, TTIP is added slowly, dropwise and the mixture is stirred for 30 min. After 30 min, the beaker is covered with aluminum foil with small holes to reduce the evaporation rate and start the peptization process by heating the solution to 85 °C, until the volume is reduced to 50 mL. To prepare the proposed two-phase system, however, a slight modification in this procedure was necessary, with the final volume reduction done at 120 °C until the volume reaches 15 mL. To this final solution, 5 mL of deionized water are added and the whole solution is stirred, capped and set aside to reach the equilibrium in phase separation. Thereafter, the solution is manipulated to control the dimension of the second phase using pipettes. The higher final heating temperature, as well as the volume reduction to 15 mL, mainly reduces the volume of isopropyl alcohol present in the solution as a co-solvent inside the semi-capped beaker (boiling point: 82.5 °C). With a lower concentration of alcohol, the added volume of deionized water does not mix with the solution, thus tending, after keeping the system at rest for a while, to separate in the desired two phases, for subsequent film deposition.

2.2. Thin film deposition

Soda-lime glass substrates are cleaned and dried, prior to use, and left in a 9:1 solution of deionized water and neutral detergent (Extran) for 24 h. Then, they are washed in deionized water for about 5 min and quickly immersed in isopropanol, being then, dried with a thermal blower. For film deposition, the substrates are attached to a substrate holder (Syringe Pump model MQBSG 1/302 connected to a controller model MQCTL 2000 MP, both from Microchemistry) that controls the dipping rate. The precursor solution is placed under the substrate in a beaker, and the substrate is then dipped at a fixed rate (10 cm/min) and removed at the same speed. After aTiO_2layer is deposited and the substrate completely removed from the solution, it is left to drain and dry for about 10 min, draining any volume of solvent in excess back to the beaker. Intermediate heat treatments are carried out between layer depositions, with the substrate being placed on a ceramic base with metal supports and introduced into an oven for 10 minutes, which is preheated and stabilized at 150 °C. At the end of the heat treatment period, the film is set aside for some time to cool down to room temperature and installed again in the substrate holder for deposition of a new layer. When the desired number of layers is reached, the sample is taken again into the oven, however, the thermal annealing process starts at room temperature and rises at a constant rate of 3°C/min, up to a target temperature of 500 °C, which is stabilized and maintained for two hours. Table 1 gives a list of prepared films and the characteristics of the two phase solution.

The chosen annealing temperature was such that the main structure formed was anatase, for its reported qualities in photocatalysis. Although the temperature interval to form anatase ranges from 300 to 700 °C[13], at 500 °C the available energy is enough to nucleate some crystallites and achieve some degree of crystallinity while not enough to start the transition to rutile.

2.3. Characterization

X-ray diffraction profiles were obtained on a Rigaku Miniflex 600 equipment, using incident Cu Kα radiation (1.54056 Å), power of 40 KV and 15 mA of current and scanning rate of 10°/min. These data were used to identify the main phase formed and evaluate the average crystallite size.

Optical characteristics of the films were obtained through optical absorption from the ultraviolet to the near infrared (250 – 1800 nm) in a Lambda 1050 UV/VIS/NIR Perkin Elmer spectrophotometer. Through this characterization it was possible to confirm reliably the phases found, as well as to analyze the stages of the photocatalysis process.

Scanning electron microscopy (SEM) measurements were performed using a Carl Zeiss scanning electron microscope, model LS15.

Table 1. Thin films prepared with distinct number of layers and height of the top phase

Thin-Film Samples	Number of deposited layers	Height of second phase (cm)
1l_0	1	Removed (N.A.)
2l_0	2	Removed (N.A.)
4l_0	4	Removed (N.A.)
1l_0.3	1	0.3
2l_0.3	2	0.3
4l_0.3	4	0.3
1l_0.6	1	0.6
2l_0.6	2	0.6
4l_0.6	4	0.6

For photocatalysis experiments, methylene blue (MB), a dye with a well-known absorption spectrum and commonly used for degradation efficiency studies[23-25] was used. In this work, this dye is diluted in deionized water, to create an aqueous solution of concentration of 2 x 10^{-3} g/L of methylene blue, or around 6 x 10^{-6} mol/L.

The TiO_2 films to be studied are, then, submerged in this solution, and are given 2 hours to adsorb particles in its surface while in darkness. At the end of these 2 hours, samples from the diluted dye are collected and an absorbance profile around 670 nm is measured for each (the maximum absorption of methylene blue is found at this wavelength[39]). After this first step, the submerged films are irradiated for 180 min with ultraviolet light from an Osram mercury lamp (11W), with emission peak at 254 nm. More samples from the diluted dye are collected at 90 min and 180 min.

To standardize and allow comparison among the studied samples and with existing literature the degradation efficiency (η) was calculated following Equation 1.

$$\eta = \left(\left(Ao - At \right) / Ai \right) * 100 \quad (1)$$

With *d* the percentage of dye degraded between the initial absorbance measurement (*Ao*) and the absorbance acquired in the respective step (*At*). The resulting data is normalized concerning the sample's area.

3. Results and Discussion

Figure 2 shows SEM images acquired for the two phase regions, and makes clear the existence of different regions in the samples deposited with the proposed two phase system, as outlined in Figure 1. The lightest area of the film (region I) during deposition is exposed only to the top phase (A), whereas the darkest area (II) comes into direct contact with the denser phase (B) and passes through the top phase. The lightest area (region I) displays sparse structures forming across the substrate's surface, having only interacted with top phase (A), it contains only a small amount of material deposited on its surface. Region II shows a higher volume of material adhered as it interacted with both phases (A and B).

SEM images reveal differences in structures formed in regions I and II, as seen in Figure 2, the inset from region I shows a sparse deposition with islands of material adhering to the substrate distant from each other, while in region II the rough surface is a consequence of two layers of deposited material and its interaction with the bottom phase (B). Despite the efforts so that the top phase (A) did not present a high concentration of TiO_2 particles, the diffusion at the interface and the turbulence created during the deposition process ensures that a number of TiO_2 particles are released from the bottom (B) to the top phase (A), where they may remain suspended. More SEM images can be seen in Figure 3 for different samples, as described in Table 1, corresponding to images taken from region I of respective films and show the presence of dispersed structures, probable result of suspended particles in the top phase (A).

The lower concentration of TiO_2 particles in the top phase (A) results in the region I described in the diagram of Figure 2, with material deposited in the form of small islands on the substrate surface. During deposition, more prominent (higher) particle structures on the substrate surface grow separated, leaving to a larger surface area, which facilitates solvent evaporation from that region. Thus, the available solvent around this region is drained in the direction of these islands by capillary forces, carrying material for the formation and further growth of such structure[30]. It results in the sparse points observable in Figures 3a to 3d for samples 1l_0.3, 2l_03, 1l_0.6 and 2l_0.6 respectively, being more branched in Figures 3b and 3d, as expected with subsequent deposited layers.

Figure 4 shows SEM images of region II of samples deposited with two layers and with varying heights for the second phase. Images show that with increasing height of the top phase (A), larger and recognizable structures become sparse as both the density and the thickness are reduced. This goes in accordance with the idea that the top phase helps "wash away" most of the adhered precursor solution back into the beaker, leading to the homogenization of some parts of the surface and growing others.

As the volume of solvent adhering to the substrate during deposition is small, due to the low viscosity and high surface tension, the drying and draining mechanisms follow a "capillarity regime"[40], which usually occurs for slower depositions. In this regime, the evaporation of solvent alters the position of the equilibrium point between the solution flux to the substrate and back to the solution. This is explained in accordance with Figure 5, where a flux diagram on the surface is drawn. Figure 5 is adapted from the work of Brinker and Hurd[29], in order to represent the flux diagram for the two phase solution method on the right side, whereas the left side represents the conventional dip-coating method, as proposed by Brinker and Hurd. Then, in the right side, the stagnation point *'s'* approaches the substrate and the surface of

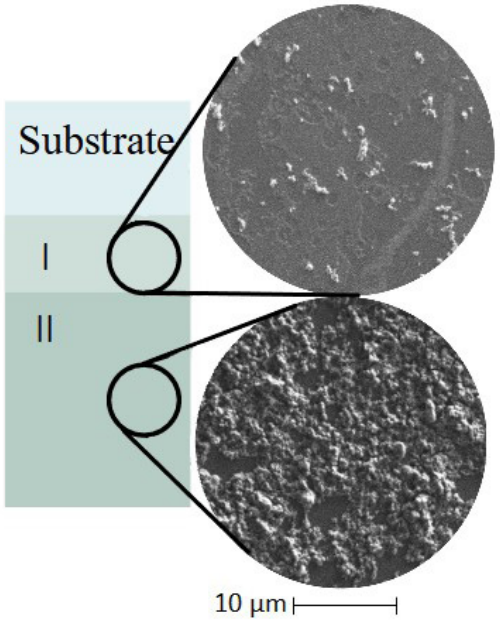

Figure 2. Diagram showing the thin film samples, and the surface SEM of the two distinct regions (Images of sample 2l_ 0.3). Image magnification: 4000x.

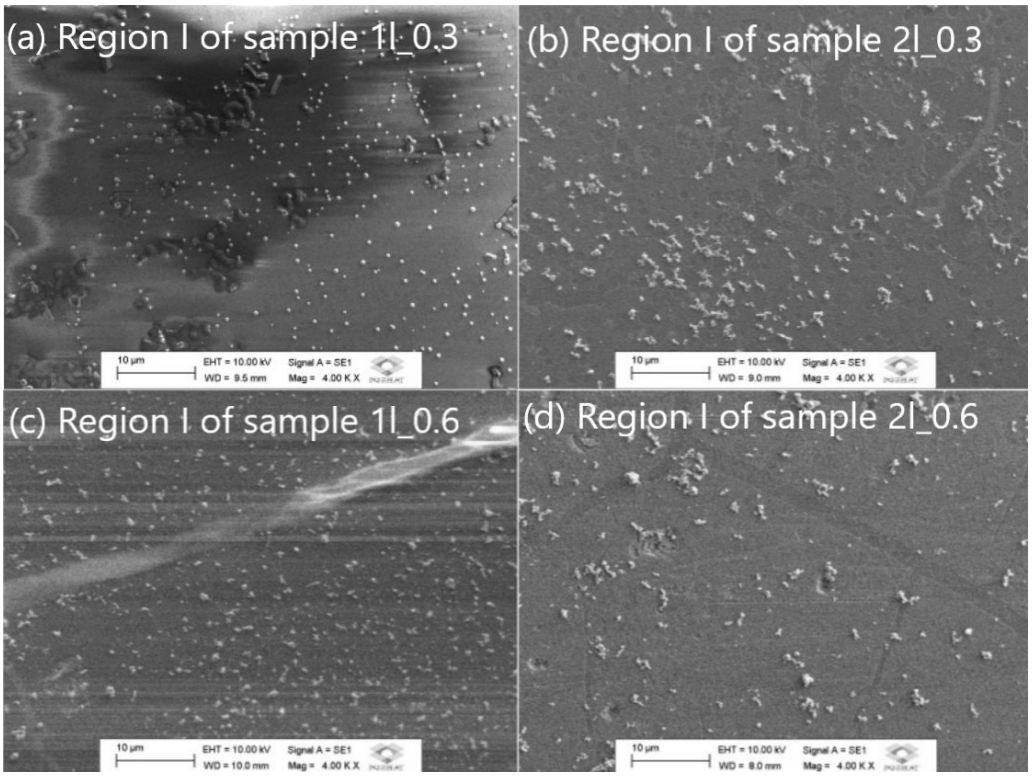

Figure 3. SEM images of films surface in regions exposed only to the top phase. Magnification 4000x

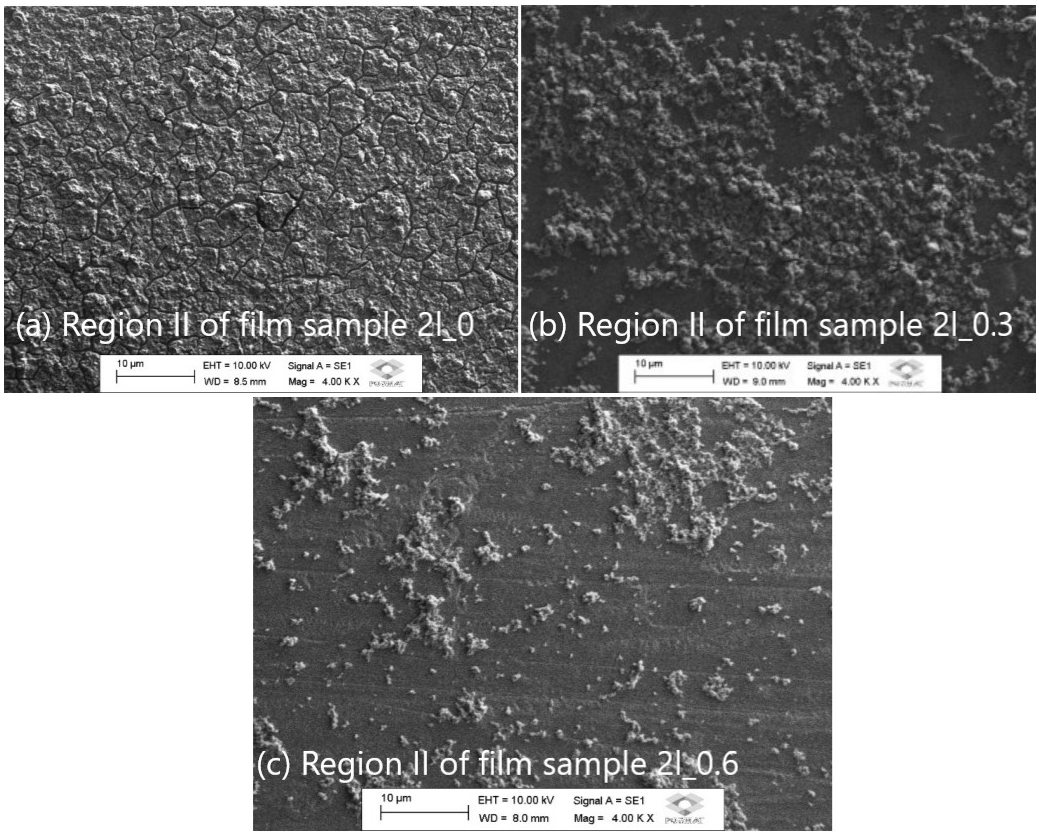

Figure 4. SEM images of region II from films deposited with 2 layers. Magnification: 4000x

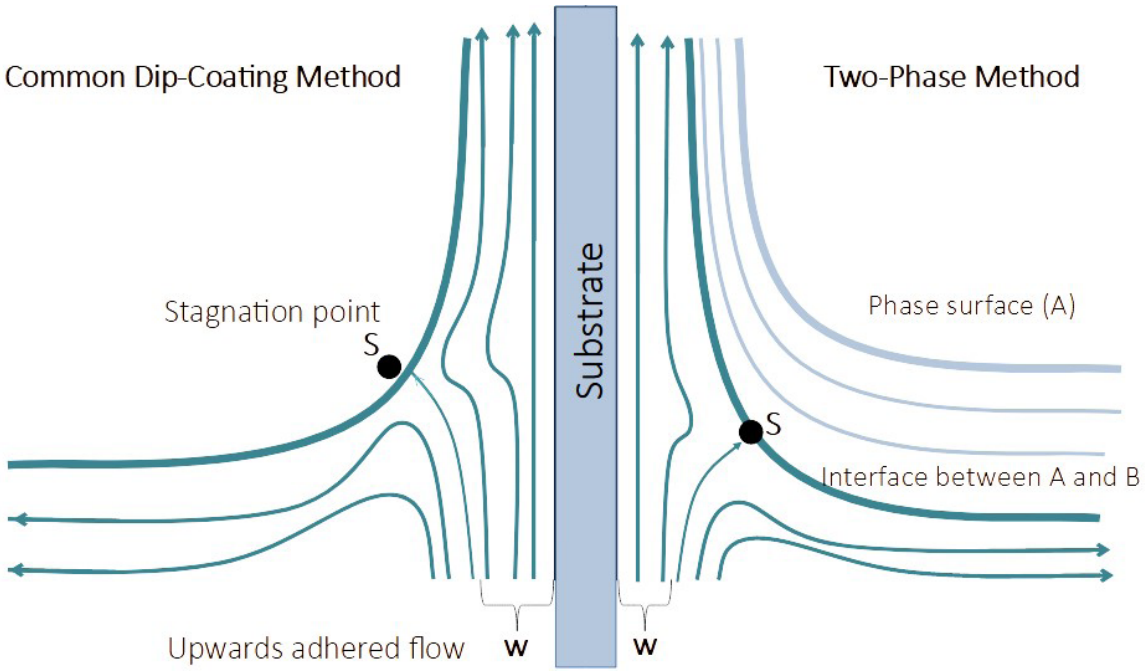

Figure 5. Flux diagram on the surface of the depositing thin film in the dip-coating process. Left: Conventional dip-coating method; Right: Two-phase method.

the precursor solution, decreasing the flow *'w'* of precursor solution to the growing film. This narrowing of flow *'w'* produces a change in the draining regime which results in the islands deposited in region I of the films. This change in flow also takes place when the top phase (A) interacts with the precursor solution, pushing most of its volume down and draining most of it back to the original recipient. It allows only a small quantity of material to adhere to the substrate.

As the substrate crosses the top phase, in the pulling step, much of the solution is removed from the substrate, and it is drained back into the beaker, due to the increased surface tension. Thus, the thickness of the deposited film can be reduced and the volume of solvent adhering to the film and the substrate maintains the regime responsible for the growth of the film structures as the capillary regime instead of the draining regime. The lower volume of adhered solvent when exposed to the atmosphere starts to evaporate easily, when compared to the higher adhered volume of solution in the conventional dip-coating method, where the time is increased to allow evaporation of the solvent. This also indicates that a lower deposition rate is not the only way to change the regime, and consequently to change the morphology and structure of films[38].

With the deposition of more layers, other interactions may take place on the film´s surface, leading to the homogenization of the regions that present varying depth, caused by defects such as fractures and cracks, which may avoid the increase in film thickness with the subsequent deposited layers. Thus, regions that carry more material during substrate removal are those with higher capillary interaction, such as cracks, wrinkles and fractures, formed by drying of previous layers, or simply rougher regions of the substrate[41].

Transmittance spectra acquired from region II of the samples are shown in Figure 6, for different samples. The effect of homogenization process may relate a lower transmittance to a higher number of layers, with films of only one layer showing less transmittance due to the growth from the capillarity regime and the diffusion of beams caused by the larger surface area. It is also in good agreement with the higher efficiency observed during photocatalysis process. From the transmittance results shown in Figures 6b and 6c it is possible to conclude that samples with a higher number of layers do not necessarily have a lower transmittance, which would be expected for samples with similar properties, deposited by the conventional dip-coating process. Images of the samples are shown in the supporting information file (Figure S1), as well as more data on transmittance and reflectance (Figure S2).

Concerning Figure 6a it is also possible to conclude that subsequent depositions did not adhere efficiently to layers already deposited, resulting in similar transmittances for samples with 1, 2 and 4 layers. The smaller amount of deposited material and the deposition of material being relegated to regions of higher capillary pressure, also prevents the deposition of subsequent layers from growing regions that have already been detached from the film[30,42]. Samples with a higher number of layers showed a superior degree of homogeneity when compared to samples deposited with 1 and 2 layers with different heights of the top phase.

X-ray diffraction measurements were performed on the surface of area II of the samples and are shown in Figure 7, regarding the predominant structures in the samples. In general, the diffraction profile showed low crystallinity, and the diffuse shape characteristic of nanoscopic crystallites domain. However, it is still possible to identify the main

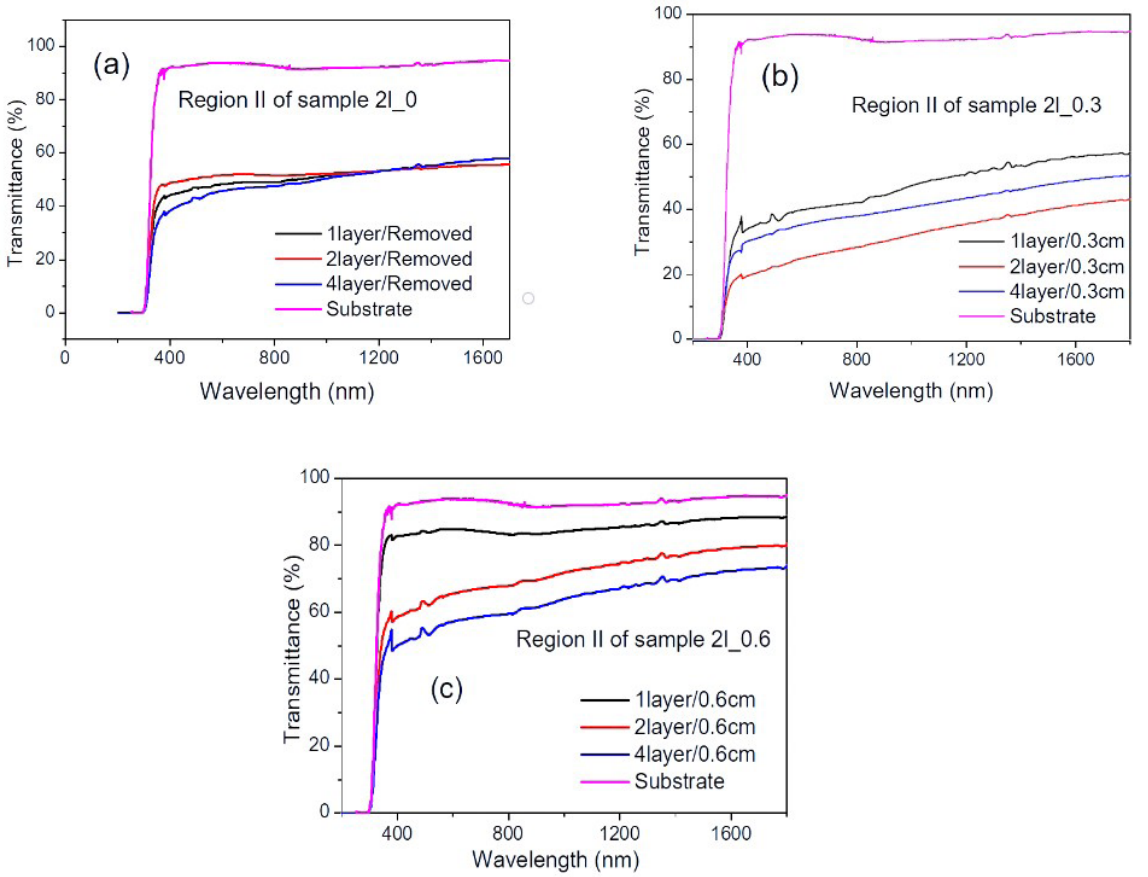

Figure 6. Transmittance spectra through region II of deposited films: (a) with the second phase removed; (b) with second phase of 0.3cm and (c) with second phase of 0.6cm.

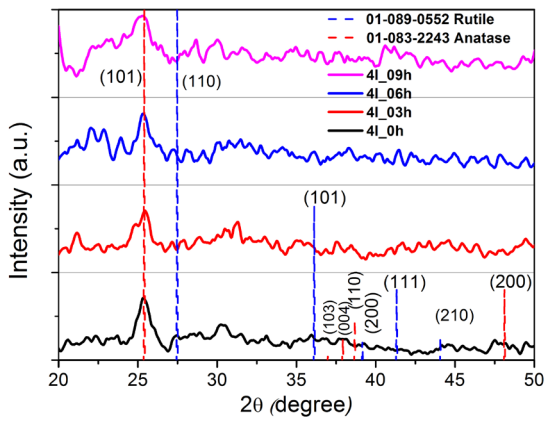

Figure 7. XRD diffractograms for samples with 4 layers

peak of the anatase structure close to 25º, referring to the plane (101) in most of the diffractograms. It is important to mention a possible presence of brookite, which is more noticeable on samples 4l_0h and 4l_03h, by the peak seen near 31°, related to plane (121), but also as a slight broadening of anatase peaks near 25° where faces (101) of anatase and (120) and/or (111) of brookite are close enough to contribute to the intensity of diffraction. Before assuming that all samples have the same predominant structure, it is necessary to take into account the parameters that can change the final deposition product. The transmittance spectra curves (Figures 6a, 6b and 6c) are used to calculate bandgap values, yielding values around 3.7 (±0.2) eV and when compared to literature values for rutile (3.0 eV) and anatase (3.3 eV)[15], it can lead us to confirm that the predominant phase in the films is anatase, following the higher bandgap values. This result is in good agreement with the X-ray data, in spite of the existence of few peaks in the diffractograms. It must be recalled that anatase is a better photocatalyst than rutile[43-46].

Table 2 shows crystallite size evaluated by the Scherrer equation[47] and lattice distortion, calculated through Equations 2 and 3 respectively.

$$S = \frac{K\lambda}{(\beta cos(\theta))} \quad (2)$$

where S is the crystallite size, K is a shape constant, taken as 0.9, λ the equipment's X-ray wavelength (Cu Kα = 0.15405 nm) and β the width at half maximum of a given peak.

$$\frac{\Delta d}{d} = \frac{\beta}{tg(\theta)} \quad (3)$$

where the distortion Δd/d given as a fraction of the width at half maximum of the most intense peak over the tangent at its diffraction angle[48].

Photocatalysis measurements were performed on film samples from the region II, which were cut from the whole sample. Figures 8a, 8c and 8e show the absorbance spectra of the aqueous solution interacting with one layered film samples and 8b, 8d and 8f films with 2 layers films, in the three steps of degradation of methylene blue: before (0 min), during (90 min) and after (180 min) the photocatalysis process, with values normalized to the original aliquot spectrum. A figure showing the absorption curves of methylene blue obtained after 180 min of photocalytic process for all the samples is given in the supporting information file (Figure S3). As expected, the shape follows the band absorbance of MB spectra. In Figure 9a the percentage of degraded methylene blue is plotted along the time axis which allows evaluating and comparing the efficiency of the different samples. To help the comparison between samples, Figure 9b shows a column chart of degradation efficiency after 180 min for different films. It can be observed that film samples deposited via the two-phase system show a higher efficiency process on breaking methylene blue molecule. According to Figure 9, samples deposited by the method described here were more efficient in general, slightly dependent on the height of the second phase, and samples with two layers were found to be more efficient than samples with only one layer. This higher efficiency is interpreted as a consequence of the large surface area of the films, achieved by the method, related to the resulting morphology from deposition (Figure 4) and changes in the surface availability and energy of the TiO_2 film[1,45,46,49].

Table 2. XRD analysis of films prepared with 4 layers of TiO_2 with varying height of second phase

Sample	Crystallite size at plane (101) (nm)	Distortion (Δd/d)
4l_09	2.94	18.1
4l_06	6.23	38.8
4l_03	3.70	23.1
4l_0	6.49	40.4

Considering the smaller volume of material used for deposition in the proposed method, and the more transparent films as inferred from the transmittance data (Figure 6c), the absorption of photons and the creation of electron-hole pairs should occur at a lower rate, as fewer photons are absorbed by the samples The same may happen with the spectra of samples deposited with a top phase of 0.3 cm (Figure 6b), if considered that a large part of the transmittance spectrum to have been scattered or reflected.

The light scattering coincides with the structures that can be observed on the SEM images of sample surface in Figure 3.These structures, through the 'capillary regime' favor growing up the substrate, creating vertical configurations.

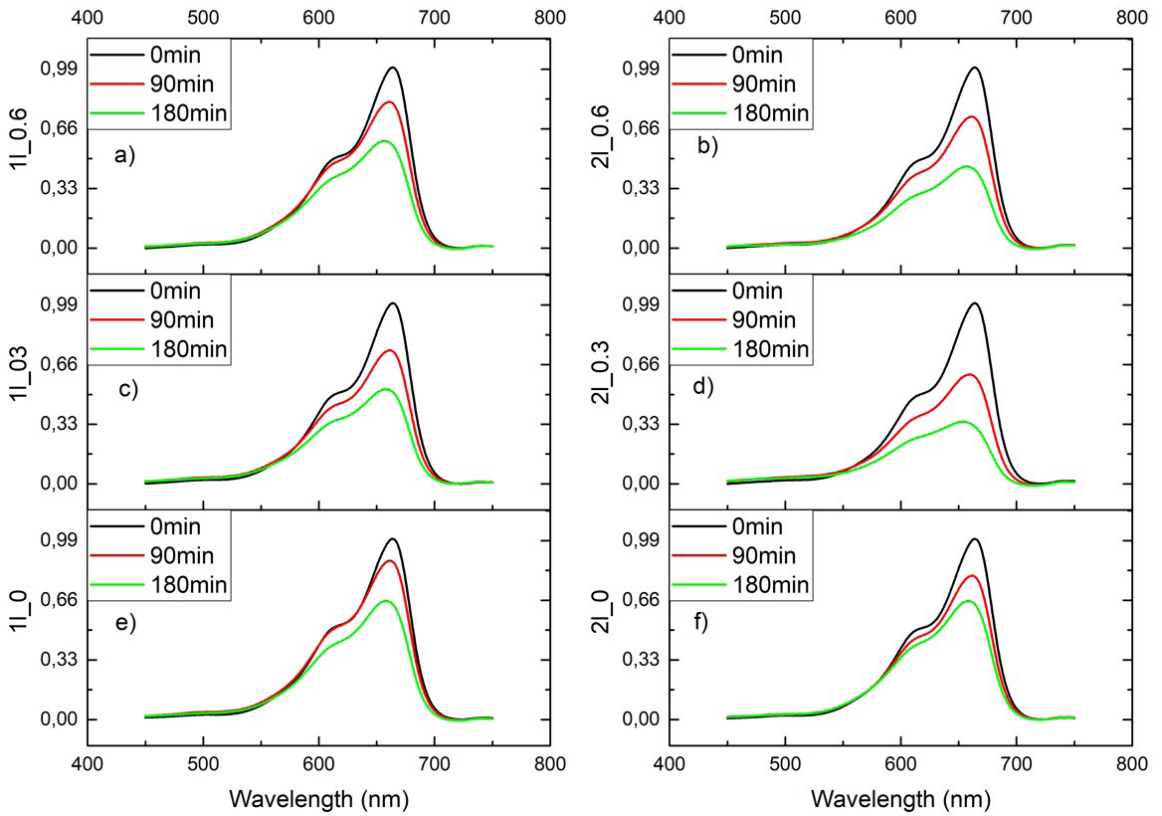

Figure 8. absorbance spectra of the aqueous solution exposed for: 0, 90 and 180 minutes in contact with film samples: a)1l_0.6; b)2l_0.6; c)1l_0.3; d)2l_0.3; e) 1l_0 and f) 2l_0

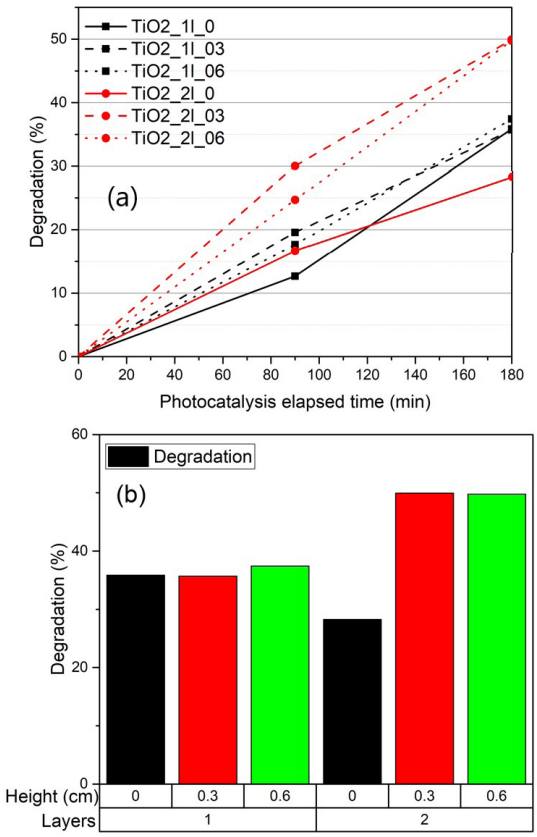

Figure 9. (a) values of peak absorbance of methylene blue along distinct time steps. The lines are just guides to the eyes; (b) Column chart that compares degradation efficiency of the photocatalysis after 180 min for different films

The higher photocatalytic efficiency can be attributed, also, to the growth of anatase, besides the low crystallinity[50], since a higher concentration of grain boundaries are related to higher surface area, and then, higher rates of oxygen, water and OH adsorption are expected[45].

The larger area created in a deposited film with lesser amount of material, is due to the concentration of deposited material in relation to the solvent. As the latter is mostly drained in the process by the pressure of the top phase, the remaining adherent to the substrate inhibits the growth of crystallites by evaporating quickly and not allowing the ramification of structures to larger areas. Following this change in morphology with increase in surface area, another possible consequence of the method that can lead to an improvement in photocatalysis efficiency, is the reorientation and exposure of different species and faces to the medium in which the film is immersed[51]. Low adsorption of methylene blue molecules was observed on the surface of the samples in general, prior to photocatalysis, since the difference in concentration of methylene blue between a control solution and solutions exposed to films kept in darkness for 2 h being around only 2% of the initially prepared solution concentration.

Another feature of the proposed method was briefly analyzed, and concerns the function of the top phase as a "cover" for the first. Assuming that the second phase is composed of a denser and more viscous phase, evaporation and solvent loss would result in the formation of a gel, difficult to deposit by the dip-coating process. Three samples of the solutions were separated, one composed only of the first phase, one composed of both, mixed, and one composed of both already separated. It was observed, during storage, that the phase separation of the second sample occurs, and as time pass, the "capped" solution by the top phase took longer to dry and turn into a gel. This is attributed to the faster loss of volume of more volatile components, such as water, alcohol and possible organic components (remnants of TTIP reactions) influenced by the atmospheric oxygen, when the sample is not capped.

4. Conclusions

The system proposed here may lead to improvements on the conventional dip-coating process concerning applications of TiO_2 thin films. The anatase main crystalline structure of the analyzed samples leads to distinct morphologic structure and optical transmittance spectra depending on the height of the top liquid solution layer. It is clear that it influences the efficiency on the degradation of methylene blue upon photocatalysis analysis.

Although the interpretation of results may be rather complex, it is possible to conclude in this work that new features on the deposition process are worth investigation, in order to adapt the method for new and for known applications, increasing efficiency. The interface created by the precursor solution in the two phase procedure deserves attention as it may lead to further developments in doping, thickness control, surface morphology and possibly more ways to further engineer thin-film properties to suit a given application.

Moreover, applications of this method can still be studied considering that it is the first time a deposition system like this is proposed. Simultaneous deposition of multiple layers, control of pH in gel formation, separation between precursor solution and air to avoid oxidation, finer control of thickness and draining regime, these are some aspects the proposed method that could be deeply investigated for and applied to. In this paper, the issues have been on changes of basic characteristics and properties.

5. Acknowledgments

This study was financed in part by the Coordenação de Aperfeiçoamento de Pessoal de Nível Superior - Brasil (CAPES) - Finance Code 001. The authors thank FAPESP (process 2019/00683-7). They also thank Prof. Fenelon M. L. Pontes by the X-ray diffraction measurements (CEPID/CDMF/Proc. FAPESP No 2013/07296-2), to Prof. José H. D. Silva by the use of the optical transmittance equipment and Prof. Carlos R. Grandini for the SEM images.

6. References

1. Nakata K, Fujishima A. TiO_2 photocatalysis: design and applications. J Photochem Photobiol Photochem Rev. 2012;13(3):169-89.
2. Zappa D, Galstyan V, Kaur N, Munasinghe Arachchige HMM, Sisman O, Comini E. Metaloxide-based heterostructures for gas sensors: a review. Anal Chim Acta. 2018;1039:1-23.

3. Zeng W, Liu T, Wang Z. Impact of Nb doping on gas-sensing performance of TiO_2 thick- film sensors. Sens Actuators B Chem. 2012;166-167:141-9.
4. Bhethanabotla VC, Russell DR, Kuhn JN. Assessment of mechanisms for enhanced performance of Yb/Er/titania photocatalysts for organic degradation: role of rare earth elements in the titania phase. Appl Catal B. 2017;202:156-64.
5. Kharel PL, Zamborini FP, Alphenaar BW. Enhancing the photovoltaic performance of dye-sensitized solar cells with rare-earth metal oxide nanoparticles. J Electrochem Soc. 2018;165(3):H52-6.
6. Peng FC, Lai Q, Zhong CY, Cui Y, Liao XJ, Liu QC, et al. Influence of ytterbium doping on the visible light photocatalytic activity of mixed phase TiO_2 nanoparticles. Key Eng Mater. 2019;807:18-25.
7. Richhariya G, Kumar A, Tekasakul P, Gupta B. Natural dyes for dye sensitized solar cell: a review. Renew Sustain Energy Rev. 2017;69:705-18.
8. Haenle M, Fritsche A, Zietz C, Bader R, Heidenau F, Mittelmeier W, et al. An extended spectrum bactericidal titanium dioxide (TiO_2) coating fo rmetallic implants: in vitro effectiveness against RSA and mechanical properties. J Mater Sci Mater Med. 2011;22(2):381-7.
9. Reszczyńska J, Grzyb T, Wei Z, Klein M, Kowalska E, Ohtani B, et al. Photocatalytic activity and luminescence properties of RE^{3+}–TiO_2 nanocrystals prepared by sol-gel and hydrothermal methods. Appl Catal B. 2016;181:825-37. http://dx.doi.org/10.1016/j.apcatb.2015.09.001.
10. Saqib N, Adnan R, Shah I. A mini-review on rare earth metal-doped TiO_2 for pho- to catalytic remediation of wastewater. Environ Sci Pollut Res Int. 2016;23(16):15941-51.
11. Mikami M, Nakamura S, Kitao O, Arakawa H, Gonze X. First-principles study of titanium dioxide: rutile and anatase. Jpn J Appl Phys. 2000;39(8B):L847-50.
12. Mikami M, Nakamura S, Kitao O, Arakawa H. Lattice dynamics and dielectric properties of TiO_2 anatase: a first-principles study. Phys Rev B Condens Matter Mater Phys. 2002;66(15):155-213.
13. Su C, Hong BY, Tseng CM. Sol-gel preparation and photocatalysis of titanium dioxide. Catal Today. 2004;96(3):119-26.
14. Zhai HJ, Wang LS. Probing the electronic structure and bandgap evolution of titanium oxide clusters (TiO_2) n-(n= 1-10) using photoelectron spectroscopy. J Am Chem Soc. 2007;129(10):3022-6.
15. Hanaor DA, Sorrell CC. Review of the anatase to rutile phase transformation. J Mater Sci. 2011;46(4):855-74.
16. Dewhurst J, Lowther J. High-pressure structural phases of titanium dioxide. Phys Rev B Condens Matter. 1996;54(6):R3673-5.
17. Kandiel TA, Robben L, Alkaim A, Bahnemann D. Brookite versus anatase TiO2 photocatalysts: phase transformations and photocatalytic activities. Photochem Photobiol Sci. 2013;12(4):602-9.
18. Zeng W, Liu T, Wang Z, Tsukimoto S, Saito M, Ikuhara Y. Oxygen adsorption on anatase TiO_2 (101) and (001) surfaces from first principles. Mater Trans. 2010;51(1):171-5.
19. Yudoyono G, Zharvan V, Ichzan N, Daniyati R, Indarto B, Pramono YH, et al. Influence of pH on the formulation of TiO2 powder prepared by co-precipitation of TiCl3 and photocatalytic activity. AIP Conf Proc. 2016;1710:030011.
20. Pelaez M, Nolan NT, Pillai SC, Seery MK, Falaras P, Kontos AG, et al. A review on the visible light active titanium dioxide photocatalysts for environmental applications. Appl Catal B. 2012;125:331-49.
21. Ijaz M, Zafar M. Titanium dioxide nanostructures as efficient photocatalyst: progress, challenges and perspective. Int J Energy Res. 2021;45(3):3569-89.
22. Nanayakkara CE, Larish WA, Grassian VH. Titanium dioxide nanoparticle surface reactivity with atmospheric gases, CO_2, SO_2, and NO: roles of hydroxyl groups and adsorbed water in the formation and stability of adsorbed products. J Phys Chem C. 2014;118(40):23011-21.
23. Kwon CH, Shin H, Kim JH, Choi WS, Yoon KH. Degradation of methylene blue via pho- tocatalysis of titanium dioxide. Mater Chem Phys. 2004;86(1):78-82.
24. Laysandra L, Sari MWMK, Soetaredjo FE, Foe K, Putro JN, Kurniawan A, et al. Adsorp- tion and photocatalytic performance of bentonite-titanium dioxide composites for methylene blue and rhodamine B decoloration. Heliyon. 2017;3(12):e00488.
25. Van Viet P, Tran HN. Adsorption and photocatalytic degradation of methylene blue by titanium dioxide nanotubes at different pH conditions. Advances in Natural Sciences: Nanoscience and Nanotechnology. 2019;10(4):045011.
26. Lazar MA, Varghese S, Nair SS. Photocatalytic water treatment by titanium dioxide: recent updates. Catalysts. 2012;2(4):572-601.
27. Xiang Q, Ma X, Zhang D, Zhou H, Liao Y, Zhang H, et al. Interfacial modification of titanium dioxide to enhance photocatalytic efficiency towards H2 production. J Colloid Interface Sci. 2019;556:376-85.
28. Nagaveni K, Hegde M, Ravishankar N, Subbanna G, Madras G. Synthesis and structure of nanocrystalline TiO_2 with lower bandgap showing high photocatalytic activity. Langmuir. 2004;20(7):2900-7.
29. Brinker CJ, Hurd AJ. Fundamentals of sol-gel dip-coating. J Phys III. 1994;4(7):1231-42.
30. Faustini M, Louis B, Albouy PA, Kuemmel M, Grosso D. Preparation of sol- gel films by dip-coating in extreme conditions. J Phys Chem C. 2010;114(17):7637-45.
31. Roberts G. Langmuir-Blodgett films. New York: Springer Science & Business Media; 2013.
32. Santos SBO, Lima JVM, Boratto MH, Scalvi LVA. Influence of substrate temperature on the deposition of the homostructure SnO_2:Sb/SnO_2:Er via sol–gel dip-coating. Ferroelectrics. 2019;545(1):10-21.
33. Ceratti DR, Louis B, Paquez X, Faustini M, Grosso D. A new dip coating method to obtain large-surface coatings with a minimum of solution. Adv Mater. 2015;27(34):4958-62.
34. Li M, An C, Pisula W, Mullen K. Alignment of organic semiconductor microstripes by two-phase dip-coating. Small. 2014;10(10):1926-31.
35. Kim YJ, Jung HT, Ahn CW, Jeon HJ. Simultaneously induced self-assembly of poly (3-hexylthiophene)(P3HT) nanowires and thin-film fabrication via solution-floating method on a water substrate. Adv Mater Interfaces. 2017;4(19):1700342.
36. Kim GW, Kim M, Park YD. Effect of solvent exchange at the biphasic dip-coating interface on the formation of polythiophene thin films. J Phys Chem C. 2018;122(4):2432-9.
37. Hanaor DA, Chironi I, Karatchevtseva I, Triani G, Sorrell CC. Single and mixed phase TiO_2 powders prepared by excess hydrolysis of titanium alkoxide. Adv Appl Ceramics. 2012;111(3):149-58.
38. Trino LD, Bronze-Uhle ES, George A, Mathew MT, Lisboa-Filho PN. Surface physico-chemical and structural analysis of functionalized titanium dioxide films. Colloids Surf A Physicochem Eng Asp. 2018;546:168-78.
39. Dinh V-P, Huynh T-D-T, Le HM, Nguyen V-D, Dao V-A, Hung NQ, et al. Insight into the adsorption mechanisms of methylene blue and chromium (iii) from aqueous solution onto pomelo fruit peel. RSC Advances. 2019;9(44):25847-60.
40. Schneller T, Waser R, Kosec M, Payne D. Chemical solution deposition of functional oxide thin films. Vienna: Springer; 2013.
41. Bartsch H, Brokmann U, Goj B, Weiss R, Radlein E, Muller J. Sol gel thin films on LTCC ceramic multilayers enable their use as thin film substrates. 2015 European Microelectronics Packaging Conference (EMPC); 2015; Deutschland. New York: IEEE; 2015. p. 1-6.

42. Brinker CJ, Scherer GW. Sol-gel science: the physics and chemistry of sol-gel processing. Saint Louis: Academic Press; 2013.
43. Luttrell T, Halpegamage S, Tao J, Kramer A, Sutter E, Batzill M. Why is anatase a better photocatalyst than rutile? Model studies on epitaxial TiO_2 films. Sci Rep. 2014;4(1):1-8.
44. Kanai N, Nuida T, Ueta K, Hashimoto K, Watanabe T, Ohsaki H. Photocatalytic efficiency of TiO_2/SnO_2 thin film stacks prepared by DC magnetron sputtering. Vacuum. 2004;74(3-4):723-7.
45. Henderson MA. The interaction of water with solid surfaces: fundamental aspects revisited. Surf Sci Rep. 2002;46(1-8):1-308.
46. Yang J, Li D, Wang X, Yang X, Lu L. Rapid synthesis of nanocrystalline TiO_2/SnO_2 binary oxides and their photoinduced decomposition of methyl orange. J Solid State Chem. 2002;165(1):193-8.
47. Patterson AL. The Scherrer formula for X-ray particle size determination. Phys Rev. 1939;56(10):978-82.
48. Spurr RA, Myers H. Quantitative analysis of anatase-rutile mixtures with an X-ray diffractometer. Anal Chem. 1957;29(5):760-2.
49. Fujishima A, Zhang X, Tryk DA. TiO_2 photocatalysis and related surface phenomena. Surf Sci Rep. 2008;63(12):515-82.
50. Zhang H, Banfield JF. Understanding polymorphic phase transformation behavior during growth of nanocrystalline aggregates: insights from TiO_2. J Phys Chem B. 2000;104(15):3481-7.
51. Ohno T, Sarukawa K, Matsumura M. Crystal faces of rutile and anatase TiO_2 particles and their roles in photocatalytic reactions. New J Chem. 2002;26(9):1167-70.

Supplementary material

The following online material is available for this article:

Figure S1 - First row: samples are prepared with only 1 layer, and, from left to right: a) without a second phase; b) with a second phase of 0.3cm; c) with a second phase of 0.6cm. Second row samples are prepared with 2 layers, and, from left to right: d)without a second phase; e) with a second phase of 0.3cm; f) with a second phase of 0.6cm.

Figure S2 - Transmittance (a) and reflectance (b) spectra for a set of samples prepared with 0, 0.3 and 0.6cm of top phase.

Figure S3 - Absorption curves of methylene blue obtained after 180 min of irradation for different samples.